
This is an electronic reprint of the original article.
This reprint may differ from the original in pagination and typographic detail.

Zhao, Wenli; Buffo, Antonio; Alopaeus, Ville; Han, Bing; Louhi-Kultanen, Marjatta

Application of the compartmental model to the gas–liquid precipitation of CO_2 - $\text{Ca}(\text{OH})_2$ aqueous system in a stirred tank

Published in:
AIChE Journal

DOI:
[10.1002/aic.15567](https://doi.org/10.1002/aic.15567)

Published: 01/01/2017

Document Version
Peer-reviewed accepted author manuscript, also known as Final accepted manuscript or Post-print

Published under the following license:
Unspecified

Please cite the original version:
Zhao, W., Buffo, A., Alopaeus, V., Han, B., & Louhi-Kultanen, M. (2017). Application of the compartmental model to the gas–liquid precipitation of CO_2 - $\text{Ca}(\text{OH})_2$ aqueous system in a stirred tank. *AIChE Journal*, 63(1), 378-386. <https://doi.org/10.1002/aic.15567>

This material is protected by copyright and other intellectual property rights, and duplication or sale of all or part of any of the repository collections is not permitted, except that material may be duplicated by you for your research use or educational purposes in electronic or print form. You must obtain permission for any other use. Electronic or print copies may not be offered, whether for sale or otherwise to anyone who is not an authorised user.

Application of the compartmental model to the gas-liquid precipitation of CO₂-Ca(OH)₂ aqueous system in a stirred tank.

Wenli Zhao*, Antonio Buffo, and Ville Alopaeus

School of Chemical Technology, Aalto University, P.O. Box 16100, FI-00076 Aalto, Finland

Bing Han, and Marjatta Louhi-Kultanen

Department of Chemical Technology, Lappeenranta University of Technology, P.O. Box 20, FI-53851, Finland

A compartmental model is formulated to assess the influence of fluid dynamics on the gas-liquid precipitation of CO₂(g)-Ca(OH)₂(aq) system in a stirred tank reactor. The model combines the description of the flow field with several sub-models, namely gas to liquid mass transfer, chemical reaction, precipitation and population balance for both gas bubbles and solid crystals. The modeling predictions, including the average volumetric mass transfer coefficient, the concentration of calcium ions, the pH of the solution and the Sauter mean diameter of the final crystal products are eventually compared with measurements carried out on a pilot-scale stirred tank. The results show that the local volumetric mass transfer rate and the final particle sizes distribution of the crystals are significantly affected by high local turbulence near the impeller. The local information simulated by the compartmental model, such as mass transfer rate, gas hold up and particle size of crystals and bubbles are important for the design and scaling of gas-liquid precipitators, with a computational time which is of several orders of magnitude faster than a full CFD computation.

Keywords: compartmental model; gas-liquid precipitation; mass transfer; population balance

* Corresponding author. Tel.: +358 45 1674316

E-mail address: zhao.wenli@hotmail.com

Present address: Aalto University, School of Chemical Technology P. O. Box 16100, FI-00076, Finland

Introduction

Gas-liquid precipitation is a widely used process in various fields such as CO₂ capture and storage, fine chemicals and gas cleaning process.¹ The ultimate process development objective is to predict and control the mass transfer rate and the size distribution of the crystal products. Such goal can be reached only if a complex model that combines different portions of the physics, namely gas-liquid mass transfer, chemical reaction, precipitation and population balance equations (PBEs) for bubbles and crystals is considered. In addition, the fluid mixing becomes crucial during the scaling up of precipitator: in fact, the non-uniform turbulent intensity locally affects the gas-liquid mass transfer rates by changing the mass transfer coefficient and specific area of the bubbles from point to point in the domain. Moreover, the precipitation kinetics including nucleation and crystal growth are in turn function of the local supersaturation, driven by the local concentration of the different chemical species.² At last, the model should properly consider that the agglomeration and breakage rate of the crystals are significantly influenced by the local values of turbulent energy dissipation in the stirred tank reactor.

For these reasons, the knowledge of the flow fields inside the equipment represents a crucial step in the model formulation. Computational fluid dynamics (CFD) is a useful tool to provide an insight into the flow fields that govern the overall precipitation rate and the crystal properties in the liquid solution.³⁻⁵ Wei and Garside⁴ for the first time coupled CFD description of the turbulent flow field with precipitation modeling for the description of a liquid phase precipitation. After this pioneering work, the CFD-PBE became a standard tool to predict the performances of industrial-scale crystallizers.⁶⁻⁸ Regarding the gas-liquid precipitation, Rigopoulos and Jones⁵ coupled a very simplified multiphase CFD model of a bubble column (i.e., assuming a monodisperse bubble distribution, without considering bubble coalescence and breakage) with a reduced PBE model for crystals with only nucleation and growth. These assumptions

may be not reasonable for stirred tank reactors, as the intensive breakage of bubbles and crystals in the vicinity of impeller will increase the gas-liquid mass transfer area and decrease the average crystal size. However, considering the development of a robust and comprehensive model that couples the multiphase flow dynamics with a detailed gas-liquid precipitation model, including mass transfer, chemical reaction, PBEs for bubbles and crystals may require a significant amount of time. It may be useful to reduce the computational costs of the CFD simulation by adopting a coarse-grained description of the fluid dynamics by means of a compartmental model.⁹⁻¹⁶ This latter approach can be beneficial to a full model development in the next step, which is the fine-tuning fitting of the numerous constants contained the different adopted sub-models.¹⁶ With this approach, CFD is only employed to obtain the hydrodynamic information, such as the flow fields, physical properties and local mixing intensity for each defined compartment. Then the physical sub-models can be solved by considering the interactions between the hydrodynamics and detailed chemical phenomena in the compartmental model.

In previous works, the compartmental model was already applied to the description of the precipitation process. Zauner and Jones¹⁰ used the compartmental model to describe the nucleation rate and the particle size in a liquid phase precipitator. Kagoshima and Mann¹¹ developed a networks-of-zones fluid mixing model to successfully predict the size distribution of BaSO₄ crystals in the unbaffled stirred vessel. Gieryz¹² reviewed several simulation methods for CaCO₃ precipitation in different types of reactors. As far as the coarse-grained description of fluid dynamics in gas-liquid systems is concerned, Laakkonen et al.¹³ described the local mass transfer rate by using the compartmental model in an agitated vessel. Nauha and Alopaeus¹⁴ combined the fluid dynamics and algal growth model in a bubble column photobioreactor by means of compartmental model. Regarding the modeling of the gas-liquid chemical adsorption process, Rigopoulos and Jones¹⁵ employed a hybrid CFD framework to investigate the chemical absorption of CO₂ bubbles into alkali solution in the bubble column. Although all these aspects

were separately investigated in many previous works, they were never brought in a single simulation tool for the simulation of a gas-liquid precipitation process. The combination of compartmental model and full gas-liquid precipitation model represents the main element of novelty of this work. With this tool, the rates of all the relevant phenomena, including gas-liquid mass transfer, chemical reaction, bubble coalescence and breakage, crystals nucleation, growth, agglomeration and breakage can be properly taken into account, together with a proper description of the turbulence intensity and the relevant mean-flow fields.

Modelling approach

As previously mentioned, a gas-liquid CFD calculation is necessary for creating the coarse-grained compartmental model. Then the flow dynamics is coupled with the sub-models accounting for the physical description of the $\text{CO}_2(g)\text{-Ca(OH)}_2(aq)$ precipitation process. The conceptual flowchart of the whole model is shown in Figure 1.

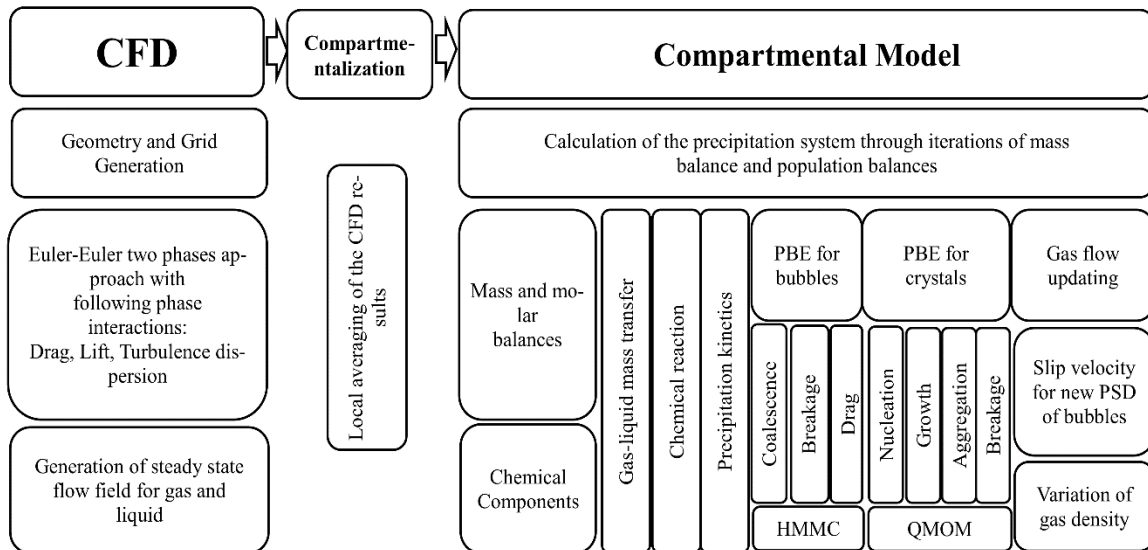


Figure 1. Flowchart of the compartmental model of gas-liquid precipitation

Assumptions

The main model assumptions are:

- 1) A single bubble size of 4 mm is assumed in the CFD calculation to obtain the initial flow field of gas, since the bubbles ranging between 1-8 mm have approximately the same terminal velocity.¹⁷
- 2) Only buoyancy, gravity and drag forces are taken into account, since they are the most important factors for determining gas holdup and bubble size distribution in stirred tank reactors.¹⁸
- 3) The crystals are assumed to follow the liquid flow because the Stokes number of the crystals (with size less than 100 μm) is generally smaller than 0.1.¹⁹ The interaction between the crystals and bubbles is neglected.
- 4) The nucleation and crystal growth rate are expressed as power-law functions of the supersaturation in the bulk solution. The crystal growth rate is taken to be independent of crystal size.

The CFD model and compartmentalization

A gas-liquid flow field is calculated in a stirred tank with Rushton turbine impeller. A sketch of the gas-liquid precipitator is reported in Figure 2(a).²⁰ The computational domain consisted of 366644 hexahedral grids. Grid independent study showed no significant variations on the properties of interest after further refinements. To calculate the CFD flow field, a steady-state two-fluid simulation was carried out with the commercial code of Fluent 16.0. The RANS approach, namely the realizable k - ε turbulence model for the mixture with standard wall functions, was adopted to predict the turbulence of the stirred tank, since it represents the only feasible way to simulate pilot-industrial scale turbulent gas-liquid systems.²¹ The degassing boundary condition was used to model the gas flowing out at the top surface of the tank.

The turbulent intensity near the impeller can be of several orders of magnitude higher than other regions in the stirred tank. Values of the mass transfer coefficient (k_L), coalescence and breakage rates for the gas bubbles, aggregation and breakage rates for the crystals, depend on the local turbulent energy

dissipation (ϵ). Therefore, the compartmentalization strategy uses the spatial distribution of energy dissipation as a reference to subdivide the domain into different areas: feeding area, stirring area, baffle area, suspension area and degassing area. An example of such division is reported in Figure 2(b). All the physical information are averaged while the flow to and from the compartments are calculated with the cell by cell algorithm.²² The number/size independence study was carried out by testing the full gas-liquid precipitation model with an increasing number of compartments from 6 to 85. The results showed that a model with 58 compartments (Figure 2(c)) is adequate to perform a number/size independent simulation.

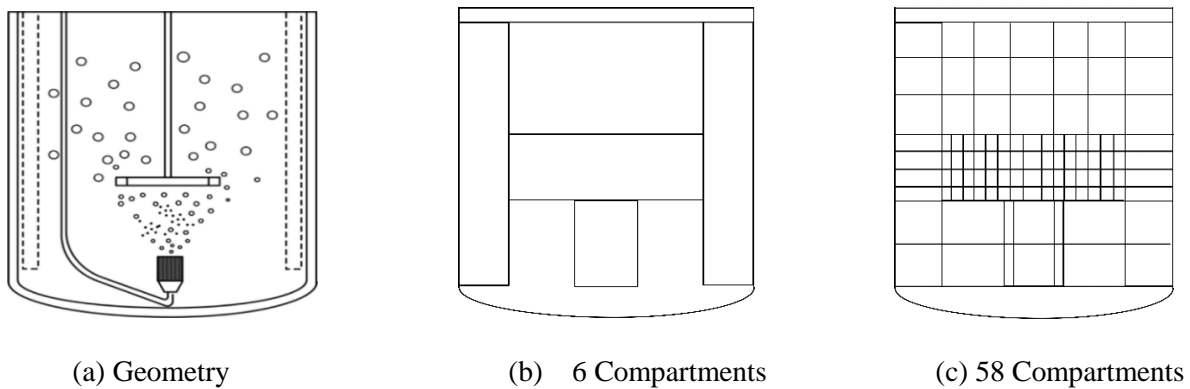


Figure 2. The schematic diagram of the geometry and compartmentalization of the stirred tank

Compartmental model

As previously mentioned, the overall mass balance and population balance of the gas phase and solid phase are coupled with several sub-models to describe mass transfer, reaction and precipitation in the compartmental model. The solution of the PBEs of bubbles is based on the high order moment method of classes (HMMC), which offers a good compromise between computational costs and accuracy.²³ Therefore, the size range of bubbles (1-20 mm) was discretized into 20 categories in this study. In order to reduce the computational load, quadrature method of moment (QMOM) was introduced to solve the PBE of crystals.²⁴ The first six moments of the crystal distributions, from m_0 to m_5 , were tracked, leading

to the calculation of three quadrature nodes. Spatial convective terms of both population balances were calculated by using the averaged information of flow in and out of the compartments.

Mass balance

The mass balance equation for each chemical specie of the liquid phase, including $\text{CO}_2(l)$, HCO_3^- , CO_3^{2-} , OH^- and Ca^{2+} in compartment i is calculated as follow:

$$\frac{dn_{L,i}}{dt} = c_{L,in}F_{L,in} - c_{L,out}F_{L,out} + \sum_{j=1}^{NB} c_{L,j}F_{L,ji} - c_{L,i} \sum_{j=1}^{NB} F_{L,ij} + N_{GL,i}A_{GL,i}V_{L,i} + r_iV_{L,i} \quad (1)$$

Terms on the right hand side are: 1) liquid feed, 2) liquid outlet, 3) internal liquid flow in, 4) internal liquid flow out, 5) mass transfer rate and 6) reaction rate. The mass transfer rate is just calculated for $\text{CO}_2(l)$. The time-average internal liquid flows were brought from previous CFD calculation and assumed to be constant in the compartmental model.¹⁴ As expected, the liquid flow is mainly driven by the movement of impeller in the stirred tank.

The mass balance equation for each chemical specie of gas phase in compartment i is calculated as follow ($\text{CO}_2(g)$ is the only specie of gas phase in this case) :

$$\begin{aligned} \frac{dn_{G,i}}{dt} = & c_{G,in}F_{G,in} - c_{G,out}A_{surface} \sum_{p=1}^{NC} v_p U_{p,slipout} Y_{p,out} \\ & + \sum_{j=1}^{NB} \left[c_{G,j}A_{ij}\varphi_j \sum_{p=1}^{NC} v_p U_{p,ji} Y_{p,j} \right] - c_{G,i} \sum_{i=1}^{NB} \left[A_{ij}\varphi_i \sum_{p=1}^{NC} v_p U_{p,ij} Y_{p,i} \right] - N_{GL,i}a_{GL,i}V_{L,i} \end{aligned} \quad (2)$$

Terms on the right hand side are: 1) Gas feed, 2) Gas outlet, 3) internal gas flow in, 4) internal gas flow out and 5) mass transfer rate. The area between the compartment i and j , A_{ij} , is the total area of the liquid flow and gas flow. Therefore, the gas hold up in the compartment, φ_G , should be taken into account when the gas flow rates between compartments are calculated. The initial gas velocity, $U_{p,ji}$, is assumed to be the same as in CFD calculation with a single bubble size. The velocities of bubbles with different size

categories are modified by incorporating the different slip velocities. Tomiyama drag force model was implemented to solve the force balance and calculate the slip velocities for the bubbles belonging to each size category.²⁵

Population balance

The discrete version of PBE for the bubbles can be written as:

$$\begin{aligned} \frac{\partial Y_{p,i}}{\partial t} = & \frac{1}{V_{disp,in}} F_{disp,in} Y_{p,in} - \frac{1}{V_{disp,out}} U_{n,slip,out} A_{surface} Y_{p,out} + \frac{1}{V_{disp,j}} \sum_{j=1}^{NB} U_{p,ji} A_{ij} \varphi_j Y_{p,j} - \frac{Y_{p,i}}{V_{disp,i}} \sum_{i=1}^{NB} U_{p,ij} A_{ij} \varphi_i \\ & + G_{p,i} + B_{p,i}^{cl} + B_{p,i}^{br} - D_{p,i}^{cl} - D_{p,i}^{br} \end{aligned} \quad (3)$$

Terms on the right hand side are: 1) Gas feed, 2) Gas outlet, 3) internal gas flow in, 4) internal gas flow out, 5) growth due to the mass transfer and varying pressure, 6) birth due to coalescence, 7) birth due to breakage, 8) death due to coalescence and 9) death due to breakage. It is worth mentioning that bubbles with different size rise with different velocities. In the compartmental model, the velocity of the bubble is calculated by summing up the liquid velocity and the bubble slip velocity referring to a single category. The slip velocities of all size categories are obtained by solving the force balances of bubbles with Newton-Raphson iteration. Then the gas flow rate of each size category is revised by updating the gas velocities. In addition, the influence of the hydrostatic pressure and mass transfer on the growth rates of bubbles are taken into account.²⁶

After applying the moment transformation, the PBE for the crystals can be written as:

$$\begin{aligned} \frac{\partial m_{k,i}}{\partial t} = & \frac{1}{V_{disp,in}} m_{k,in} F_{disp,in} - \frac{1}{V_{disp,out}} m_{k,out} F_{disp,out} + \frac{1}{V_{disp,j}} \sum_{j=1}^{NB} m_{k,j} F_{disp,ji} - \frac{1}{V_{disp,i}} m_{k,i} \sum_{j=1}^{NB} F_{disp,ij} \\ & + G_{k,i} + N_{k,i} + B_{k,i}^{ag} + B_{k,i}^{br} - D_{k,i}^{ag} - D_{k,i}^{br} \end{aligned} \quad (4)$$

Terms on the right hand side are: 1) crystals feed, 2) products outlet, 3) internal crystals flow in, 4) internal crystals flow out, 5) growth term, 6) nucleation term, 7) birth due to agglomeration, 8) birth due to breakage, 9) death due to agglomeration and 10) death due to breakage. The Wheeler algorithm is used to calculate the quadrature approximation from the set of the transported moments.²⁷

Table 1. Initial process parameters and physical properties of system

Initial parameters	Values
Initial concentration of $\text{Ca}(\text{OH})_2(\text{aq})$	20.32 mol/m ³
Volume of the dispersion	2.64×10 ⁻³ m ³
Concentration of $\text{CO}_2(\text{g})$ in the feed gas	100 volume %
Gas feeding rate	1.67×10 ⁻⁵ m ³ /s
Impeller speed	58.64 rad/s
Temperature	25°C
Diffusion coefficient of $\text{CO}_2(\text{g})$	1.91×10 ⁻⁹ m ² /s
Dynamic viscosity of liquid	8.90×10 ⁻⁴ Pa·s
Density of mixture	997.22 kg/m ³

Physical sub-models

The gas-liquid precipitation of the $\text{Ca}(\text{OH})_2(\text{aq})\text{-CO}_2(\text{g})$ system consists of mass transfer of $\text{CO}_2(\text{g})$, the reaction between the hydroxyl ion and $\text{CO}_2(\text{l})$, and the precipitation of CaCO_3 . The initial parameters are listed in Table 1. The gas-liquid mass transfer coefficient in each compartment can be correlated by the following equation, based on the surface renewal theory:²⁸

$$k_{L,i} = \frac{2}{\sqrt{\pi}} \sqrt{D_{\text{CO}_2}} \left(\frac{\varepsilon_i \rho_L}{\mu_L} \right) \quad (5)$$

The specific mass transfer area is obtained from the BSD calculated by population balance model. The bubble coalescence and breakage mechanisms are assumed to be caused by turbulent fluctuations, and standard closures for air-water systems in the stirred tank were adopted.¹³ The initial bubble size was assumed the same as in the CFD calculation. The feed bubble size was set to be 3mm with a standard deviation of 1mm, as estimated by the correlation of Kazakis et al.²⁹ for porous gas sparger in the experiment. The reaction model for hydroxyl ion with CO₂(l) developed by Cents et al.³⁰ was adopted. The calcium ions along with the carbonate anions produced by the reaction provide the supersaturation for the precipitation.

In the precipitation model, nucleation, crystal growth, agglomeration of crystals and breakage of agglomerates were taken into account. The power-law functions are commonly used to calculate the nucleation rate as well as the growth rate:

$$N = k_n \left(\sqrt{[Ca^{2+}][CO_3^{2-}]} - \sqrt{K_{sp,CaCO_3}} \right)^\alpha \quad (6)$$

$$G = k_g \left(\sqrt{[Ca^{2+}][CO_3^{2-}]} - \sqrt{K_{sp,CaCO_3}} \right)^\beta \quad (7)$$

The nucleation constant could be influenced by several parameters, such as energy dissipation, suspension density, temperature, surface tension and viscosity of liquid. However, the detailed description of the nucleation mechanism is out of the scope of this work. Therefore, the precipitation kinetics were taken from the literatures.^{31, 32} Outcome of the precipitation process, namely the particle size distribution, can be significantly influenced by the occurrence of agglomeration of crystals and breakage of agglomerates, which are caused by the turbulence fluctuations. The agglomeration rate consists of collision rate and collision efficiency:³³

$$R_{ag}(L_i, L_j) = \left(\frac{2k_B T}{3\mu} \frac{(L_i + L_j)^2}{L_i L_j} + 1.29 \left(\frac{\varepsilon}{\nu} \right)^{1/2} (L_i + L_j)^3 \right) \Psi \quad (8)$$

The first term inside the brackets accounts for the Brownian collisions, while the second the turbulence-induced collisions. The collision efficiency ψ was estimated by using the model proposed by Hounslow et al.³⁴

$$\Psi = \frac{(\Omega(\varepsilon)/\Omega_{50})^\Gamma}{1 + (\Omega(\varepsilon)/\Omega_{50})^\Gamma} \quad (9)$$

The strength of aggregate, $\Omega(\varepsilon)$, is a function of the energy dissipation, crystal size, apparent yield stress, density of particle, dynamic viscosity of liquid and the growth rate of crystal. M_{50} and Γ are parameters fitted against experimental data.

The particle breakage is assumed to be caused by two mechanisms: normal stresses acting on the surface of the particle and disrupting stresses acting on a particle trapped between two eddies.²⁷ Different mechanisms prevail depending on the ratio between the particle size and the size of smallest turbulence eddy. The breakage is likely to occur by means of the normal stresses when the size of particle is larger than the size of the eddy. For particles of sizes smaller than the turbulent microscale, the breakage is likely to be caused by the shear stress originating from the turbulent velocities of different eddies acting on the opposite sides of the particle. The most often used agglomerate breakage rate model is based on a formulation, where the breakage rate is assumed to be a power law function of kinematic viscosity, turbulence dissipation, and agglomerate size.^{33,35} Due to dimensional considerations, the powers in this model are not independent. Based on dimensional consistency, the breakage law can be re-organized in terms of well-known quantities, namely the ratio between the diameter of the agglomerate (L) and the Kolmogorov length scale (η), and Kolmogorov time scale (η_T). With these quantities, the breakage rate can be written as follows:

$$R_{br} = c_{br} \left(\frac{L}{\eta} \right)^\gamma \eta_T^{-1} \quad (10)$$

where c_{br} is a dimensionless empirical constant as well as the exponent γ . This exponent is the same as reported earlier³⁵ for power law models for agglomerate size dependency, and the pre-exponential factor is also the same. This formulation of the well-established power law breakage rate is automatically dimensionally correct, and also reveals underlying dependencies between turbulent micro-scales, agglomerate size, and agglomerate breakage rate. By comparing the experimental and modeling results, 1.5×10^{-4} and 1 were chosen for c_{br} and γ respectively, which are in line with values given by other researchers in the literature.³⁶ The fragmentation was assumed to be uniform as a first approximation.

Results and discussion

CFD and compartmentalization

The quality of the compartmentalization can be assessed through the comparison of the flow field calculated with the CFD and that given by the compartmental model. The most important results are the distribution of energy dissipation (ε) and gas hold up (φ_G). The results of the compartmental model with only flow field and population balance of bubbles at steady state are shown in Figure 3, together with CFD calculations. The comparison shows that compartmentalization with 58 compartments can preserve the characteristic of the flow fields, since both the local and maximum value of ε and φ_G are in the same range of CFD calculation.

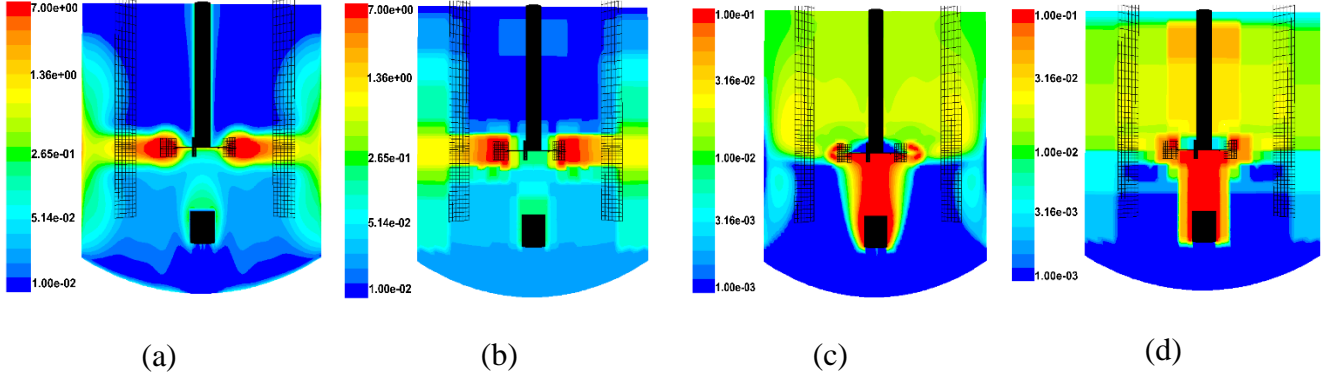


Figure 3. Energy dissipation (ε), W/kg and gas hold up (φ_G): (a) ε in CFD calculation; (b) ε in compartmental calculation; (c) φ_G in CFD calculation; (d) φ_G in compartmental calculation

It is important to mention that the average $\bar{\varepsilon}$ is 0.26 W/kg in the CFD calculation, however, according to a well-known correlation,³⁷ the $\bar{\varepsilon}$ under the concerned operating condition should be near 0.4 W/kg. The reason of this mismatch stems on the k - ε turbulent model, or more in general on RANS models, which are known to underestimate the total turbulent energy dissipation.^{38,39} In this case, a possible workaround is to scale the values of ε in the compartments to match the value of $\bar{\varepsilon}$, as different sub-models depend on local value of turbulent dissipation rate. Therefore the torque moment calculated by CFD was introduced to scale the turbulent dissipation values in the compartment model:³⁹

$$\varepsilon_L = \frac{2\pi N_s |M|}{\rho_L V_L} \quad (11)$$

It is also important to compare the global gas hold-up between compartmental model and CFD: the compartmental model predicted a value of 1.06% in contrast to 0.97 % of the CFD calculation. This slight difference could be caused by the calculation of PBEs of bubbles. In fact, the initial bubble diameter in the preliminary CFD simulation is assumed to be 4 mm, while the value of the bubble diameter can change during the compartmental model simulation due to the solution of the PBEs, leading to a size distribution of bubbles with an average diameter of 3.96 mm.

Experimental validation

Measurements of the steady state volume average k_{LA} on the investigated system were already carried out,⁴⁰ while the dynamic concentration of calcium, $[Ca^{2+}]$, and the pH of the solution under different operating conditions were performed in this work. $[Ca^{2+}]$ of the sample was measured by ion chromatography (ICS-1100 from Thermo Scientific Inc.), while a pH meter (Metrohm 744) was used to monitor in situ the pH of the solution during the gas-liquid precipitation.

The steady state volume average k_{LA} calculated by the compartmental model under various operating conditions are compared with experimental results in Table 2. As one may note, the agreement is very good under different operating conditions, meaning that the compartmentalization strategy and set of sub-models are adequate to describe the system.

Table 2. Experimental validation of the steady state k_{LA}

N , rad/s	Q , m ³ /s	k_{LA} (Experiment), s ⁻¹	k_{LA} (Modeling), s ⁻¹
58.64	1.67×10^{-5}	0.0196	0.0189
68.06	1.67×10^{-5}	0.0304	0.0289
78.53	1.67×10^{-5}	0.0452	0.0427
58.64	8.35×10^{-5}	0.0345	0.0333

As the flow field in a stirred tank is significantly affected by the rotation of impeller, $[Ca^{2+}]$ and pH under different impeller rates were simulated and compared with the experimental data. The results of such comparison are reported in Fig 4. As it is possible to observe, the higher impeller speed increases the precipitation rate: during the nucleation period (namely the first few seconds of the process), $[Ca^{2+}]$ remains constant because the critical size of the crystal nucleus is assumed to be $0.01\mu\text{m}$, which is too

small to have obvious contribution to the amount of CaCO_3 . After approximately 90s instead, when the concentration reaches the lowest value, $[\text{Ca}^{2+}]$ tends to increase slightly again since further decreasing of the pH caused by gas feeding may lead to the dissolution of crystals. The dissolution model has not been considered because the crystal dissolution is out of the scope of this work. The influence of impeller rate on the evolution of pH is similar with that on the $[\text{Ca}^{2+}]$ in Fig 4(b). pH of the solution is determined by the gas-liquid mass transfer rates and the consequent reaction between $\text{CO}_2(l)$ and OH^- . The higher impeller speed leads to the increase of average energy dissipation in the stirred tank, enhancing the mass transfer rates. Moreover, the pH begins to drop dramatically when the precipitation stops. As a key parameter dominating the main species including $\text{CO}_2(l)$, HCO_3^- and CO_3^{2-} in the $\text{CO}_2(g)\text{-H}_2\text{O}(l)$ equilibrium system, pH can be used to estimate and monitor the overall precipitation time.

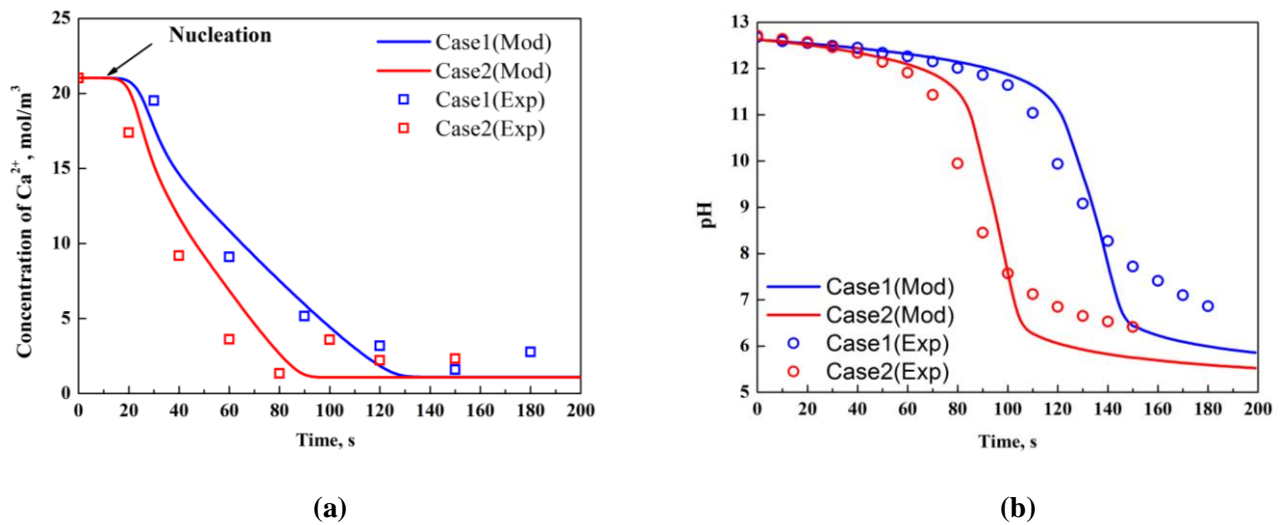


Figure 4. The revolution of $[\text{Ca}^{2+}]$ and pH. Case1: $N= 36.65 \text{ rad/s}$; $Q = 1.67 \times 10^{-5} \text{ m}^3/\text{s}$; Case2: $N= 58.64 \text{ rad/s}$; $Q = 1.67 \times 10^{-5} \text{ m}^3/\text{s}$.

The influence of the impeller rate on the mean Sauter diameter of the crystals is reported in Table 3. As can be clearly seen, d_{32} of crystals decreases when the impeller rate increases from 36.65 rad/s to 58.64 rad/s, as one may expect due to the prevailing of particle breakage over agglomeration at higher impeller rates.

Table 3. The influence of impeller rate on the d_{32} of final crystal products (at 150s)

N , rad/s	Q , m ³ /s	d_{32} (Exp), μm	d_{32} (Mod), μm
36.65	1.67×10^{-5}	8.86	7.24
58.64	1.67×10^{-5}	2.24	2.56

Local information of the stirred tank

The gas-liquid mass transfer rate is typically the rate limiting step of the overall precipitation process. However, the rate limiting step was reported to be significantly affected by the local flow dynamics.⁴¹ To address this issue, a time scale analysis was performed by calculating the characteristic time scales of gas-liquid mass transfer, micro mixing, nucleation and crystal growth for the operating condition with impeller rate of 58.64 rad/s and gas flow rate of 1.67×10^{-5} m³/s. It is important to note that the time scales are not constant during the precipitation process; especially the time scales of crystal nucleation and growth are both varying from 0.001 s to infinite, as supersaturation and growth rates approach zero when the precipitation stops (after approx. 90s as can be seen in Fig 4(a)). Regarding the mass transfer and the mixing time scales instead, they ranged respectively between 1-100 s and 0.0001-0.01 s, showing why the mass transfer rate can be considered as a the rate limiting step of the process. In order to understand the influence of local flow field on the gas-liquid precipitation, the local information of case 2 was presented.

As it is shown in Figure 5(a), the average gas volume fraction, $\bar{\varphi}_G$, decrease quickly during the first few seconds. In a similar case, Darmana et al.⁴² reported that the $\bar{\varphi}_G$ decreased by 40%-60% in the chemical absorption of CO₂ into NaOH solution. This is mainly due to the bubble shrinking caused by the CO₂ transferring from the gas to the liquid phase. It is worth noticing that the average gas volume fraction

starts to increase rapidly with time after 90s. The experimental and modeling results of $[Ca^{2+}]$ show that the precipitation stops at 90s in Fig 4(a). Then the accumulation of $CO_2(l)$ will reduce the driving force of gas-liquid mass transfer, which leads to the increase of gas volume fraction with time.

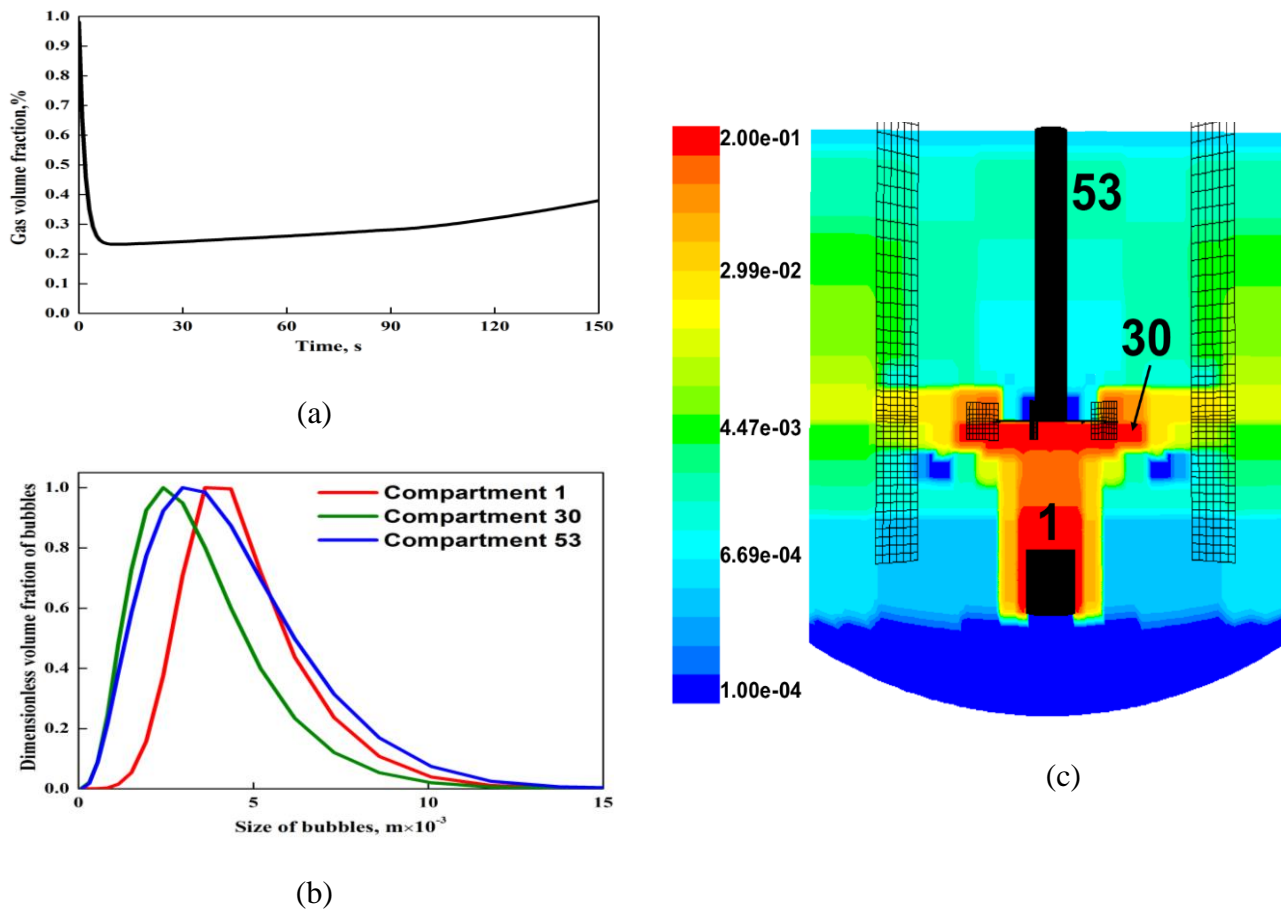


Figure 5. The gas volume fraction, BSD and local k_{La} . (a) The average ϕ_G , %; (b) BSD; (c) k_{La} , s⁻¹

In order to understand the behavior of the gas-liquid mass transfer during the precipitation, the local bubble size distribution (BSD) and k_{La} at 30s are presented. The different BSD in different compartments are shown in Figure 5(b). As can be seen, the bubbles in compartment 1 are largest because coalescence phenomenon is prevailing in the feeding area due to the high gas volume fraction. The bubble distribution in compartment 30 is shifted towards small diameters since the breakage and mass transfer are prevailing in the impeller area due to the high turbulent intensity. In the suspension area, the size of bubbles is mainly determined by the combined action between coalescence and mass transfer. Therefore, bubbles

located in compartment 53 near the surface have average size in between these two extremes with a wider size distribution. Figure 5(c) shows instead the spatial profile of k_{La} in the reactor. As it can be observed, the flow field has a strong influence on the local mass transfer rate: the larger values of k_{La} are in the feeding area where the local φ_G is higher. The intensive breakage of bubbles in the impeller area can increase k_L and a significantly as well.

The final crystal size distribution (CSD) is the result of the concurrent actions of several phenomena, as nucleation, growth, agglomeration and breakage. The driving force of the precipitation is known to be the supersaturation, which is the key parameter in the calculation of crystal nucleation, crystal growth and agglomeration. The supersaturation is mainly determined by the chemical absorption of CO_2 into the $\text{Ca}(\text{OH})_2$ solution and the flow field of liquid phase. In order to show the local precipitation rate, the evolution of local supersaturation with time is shown in Figure 6.

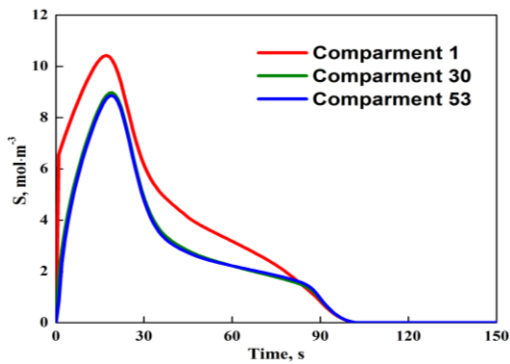


Figure 6. The local supersaturation

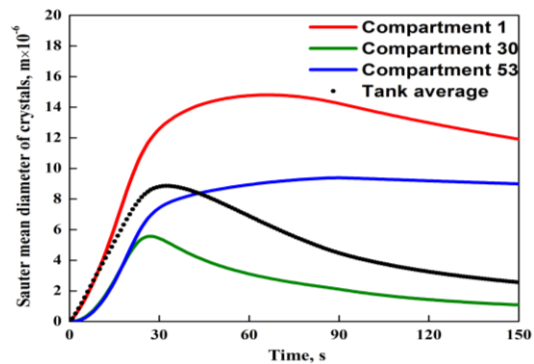


Figure 7. The local d_{32} of crystals.

The evolution of supersaturation is faster in feeding region, such as compartment 1, due to the high mass transfer rate. The difference of local supersaturation in other regions of the tank is quite small because the mixing of liquid is uniform due to the high impeller rate. Therefore, the local growth rate and nucleation rate should be similar in agreement with the assumption 4. The final CSD is mainly decided by the breakage and agglomeration in the compartmental model.

The local Sauter mean diameter, d_{32} , of the crystals calculated as the ratio of the 3th and 2nd-order moments is shown in Figure 7, together with the volume-averaged d_{32} . The volume-averaged d_{32} is obtained by counting the crystals in all of the compartments. In this case, the average d_{32} is influenced by the competition of nucleation, growth, agglomeration and breakage: the nucleation, growth and agglomeration are prevailing before 25s, corresponding to the highest value of supersaturation reached by the system. Then the breakage of larger agglomerates leads to the decrease of average d_{32} , following the decrease of the supersaturation after 25s. It is clearly shown that the stronger turbulence will lead to earlier decrease of d_{32} and small crystals size, since the breakage frequency is a function of energy dissipation and the size of agglomerates. In addition, the supersaturation vanishes at about 90s when the pH drops. Further gas feeding after this point is not beneficial as may cause CO₂ accumulation and consequent crystal dissolution.

In the view of above discussion, the combination of flow field and complex sub-models is necessary in the simulation of gas-liquid precipitation, as neglecting the interactions between the flow field and bubbles/particles dynamics may cause large errors during the design and scaling up of these processes. The compartment model represents a cheap alternative to full CFD simulations, since it is capable of coupling the flow dynamics and the interconnected sub-models, allowing also to the evaluate the effect of operating parameters that do not modify the fluid field such as the purity of CO₂(g) and the initial concentration of Ca²⁺, without any additional CFD calculations.

Conclusion

This paper introduces the compartmental model to estimate the influence of the fluid dynamics on the gas-liquid precipitation in a pilot-scale stirred tank. This approach inherently combines the local fluid field with complex sub-models including mass transfer, chemical reaction, precipitation and population balance for bubbles and crystals. Compartmentalization is performed from a steady state two-fluid CFD

calculation by considering the spatial distribution of turbulent dissipation. The physical sub-models are integrated together with the flow field description in the compartmental model.

The flow dynamics has a strong influence on the local mass transfer coefficient and the particle size distribution of crystals. Due to the low computational costs compared to a full CFD simulation, the compartmental model allows time-consuming operations, such as the fine-tuning fitting of the sub-model parameters. With further experimental investigations, several model parameters in the sub-models can be fine-tuned and used to scale-up the process. By appropriate division of the fluid domain, the compartmental model can also be used to successfully model gas-liquid precipitation process in different geometries.

Acknowledgments

Financial support from the Finnish Academy, project FLUKI (no. 13259597, no. 260141) is gratefully acknowledged

Notation

α	=	exponent of nucleation
β	=	exponent of growth
γ	=	exponent for particle size in power-law breakage kernel
ε	=	turbulent energy dissipation
μ	=	dynamics viscosity
ρ	=	density
φ	=	gas hold up in each compartment
ψ	=	collision efficiency
Ω	=	strength of aggregate

η	=	Kolmogorov length scale
η_T	=	Kolmogorov time scale
c	=	concentration of component
aq	=	aqueous solution
B	=	birth function
D	=	death function
D_{CO_2}	=	diffusion coefficient of carbon dioxide in the liquid
F_{ij}	=	liquid flow rate from compartment i to compartment j
g	=	gas phase
G	=	growth term of bubbles and crystals
K_{sp}	=	solubility product
k_n	=	nucleation rate constant
k_g	=	growth rate constant
l	=	liquid phase
m_k	=	the k-th moment of crystals
M	=	torque of the impeller
n	=	amount of component
N	=	nucleation term of crystals
N_s	=	impeller speed
NB	=	total number of compartments
NC	=	total number of bubble size categories
N_{GL}	=	flux of gas-liquid mass transfer
r	=	reaction rate
R	=	agglomeration and breakage rate
S	=	supersaturation

U_{ij} = gas velocity from compartment i to compartment j
 V = volume of compartment
 v = volume of single bubble of each category
 Y = bubble number density

subscripts

ag = agglomeration
br = breakage
cl = coalescence
disp = dispersion
G = gas phase
i, j = index of compartment
in = index of the feeding compartment
k = index of the moment
L = liquid phase
out = index of the flow out compartment
p = index of bubble size category
slip = slip velocity

Literature Cited

1. Al-Rashed MH, Jones AG. CFD modelling of gas-liquid precipitation. Chem Eng Sci. 1999;54:4779-4784.
2. Myerson AS. Handbook of industrial crystallization (2nd edition). Woburn: Butterworth-Heinemann, 2001.
3. Ali BA, Janiga G, Temmel E, Seidel-Morgenstern, Thevenin D. Numerical analysis of hydrodynamics and crystal motion in a batch crystallizer. J. Cryst. Growth. 2013;372:219-229.
4. Wei H, Garside J. Application of CFD modelling to precipitation systems. Chem Eng Res Des. 1997;75(2):219-27.

5. Rigopoulos S, Jones AG. Dynamic modelling of a bubble column for particle formation via a gas-liquid reaction. *Chem Eng Sci.* 2001;56:6177-6184
6. Woo XY, Tan RBH, Chow PS, Braatz RD. Simulation of mixing effects in antisolvent crystallization using a coupled CFD-PDF-PBE approach. *Cryst. Growth. Des.* 2006;6:1291-1203.
7. Cheng J, Yang C, Mao, ZS. CFD-PBE simulation of premixed continuous precipitation incorporating nucleation, growth and aggregation in a stirred tank with multi-class method. *Chem Eng Sci.* 2012;68(1):469-480.
8. Mao ZS, Yang C. Numerical solution of multiphase reactors with continuous liquid phase (1st edition). Oxford: Chemical Industry Press, 2014.
9. Patterson GK. Simulating turbulent field mixers and reactors-or-taking the art out of the design. *Turbulence in Mixing Operations* (1st edition). New York: Academic Press, 1975.
10. Zauner R, Jones AG. On the influence of mixing on crystal precipitation processes—application of the segregated feed model. *Chem Eng Sci.* 2002;57(5):821-831.
11. Kagoshima M, Mann R. Development of a networks-of-zones fluid mixing model for an unbaffled stirred vessel used for precipitation. *Chem Eng Sci.* 2006;61:2852–2863.
12. Gierycz P. Simulation of CaCO₃ crystal growth in multiphase reaction. In: Kolesnikov and Borisenko. *Modern aspects of bulk crystal and thin film preparation*(1st edition). Rijeka: InTech,2012:555-78.
13. Laakkonen M, Moilanen P, Alopaeus V, Aittamaa J. Modelling local gas - Liquid mass transfer in agitated vessels. *Chem Eng Sci.* 2007;85(5):665-675.
14. Nauha EK, Alopaeus V. Modeling method for combining fluid dynamics and algal growth in a bubble column photobioreactor. *Chem Eng J.* 2013;229:559–568.
15. Rigopoulos S, Jones A. A hybrid CFD-reaction engineering framework for multiphase reactor modelling: basic concept and application to bubble column reactors. *Chem Eng Sci.* 2003;58:3077–3089.
16. Laakkonen M, Alopaeus V, Aittamaa J. Validation of bubbles breakage, coalescence and mass transfer models for gas-liquid dispersion in agitated vessel. *Chem Eng Sci.* 2006;61:218-228.

17. Clift R, Grave JR, Weber ME. Bubbles, Drops and Particles (1st edition). New York: Academic Press, 1978.
18. Lane, GL, Schwarz MP, Evans GM. Numerical modelling of gas-liquid flow in stirred tanks. Chem Eng Sci. 2005;60(8-9):2203-2214.
19. Tropea C, Yarin A, Foss JF. Springer Handbook of Experimental Fluid Mechanics (1st edition). New York: Springer-Verlag Berlin Heidelberg, 2007.
20. Han B, Qu HY, Niemi H, Sha ZL, Louhi-Kultanen M. Mechanistic study of magnesium carbonate semibatch precipitation with magnesium hydroxide and CO₂. Ind Eng Chem Res. 2014;53(30):12077-12082.
21. Buffo A., Marchisio DL. Modeling and simulation of turbulent polydisperse gas-liquid systems via the generalized population balance equation. Rev Chem Eng. 2014;30(1):73-126.W
22. Nauha EK, Alopaeus V. Modeling outdoors algal cultivation with compartmental approach. Chem Eng J. 2015;259 : 945–960.
23. Alopaeus V, Laakkonen M, Aittamaa J. Solution of population balances with breakage and agglomeration by high-order moment-conserving method of classes. Chem Eng Sci. 2006; 61:6732–6752.
24. Marchisio DL, Pikturna JT, Fox RO, Vigil RD, Barresi AA. Quadrature method of moments for population balances with nucleation, growth and aggregation. AIChE J. 2003;49:1266–1276.
25. Tomiyama A; Kataoka I; Zun I; Sakaguchi T. Drag coefficients of single bubbles under normal and micro gravity conditions. JSME Int J., Ser. B. 1998;41(2):472-479.
26. Laakkonen M. Development and validation of mass transfer models for the design of agitated gas-liquid reactors, Ph.D. Thesis. Helsinki University of Technology. ESPOO, 2006.
27. Marchisio DL; Fox RO. Computational models for polydisperse particulate and multiphase systems (1st edition). New York: Cambridge University Press, 2013.
28. Lamont JC, Scott DS. An eddy cell model of mass transfer into the surface of a turbulent liquid. AIChE J. 1970;16(4):513-519.

29. Kazakis NS, Mouza AA, Paras SV. Experimental study of bubble formation at metal porous spargers: Effect of liquid properties and sparger characteristics on the initial bubble size distribution. *Chem Eng Sci.* 2008;137(2): 265-281.
30. Cents AHG, Brillman DWF, Versteeg GF. CO₂ absorption in carbonate/bicarbonate solutions: The Danckwerts-criterion revisited. *Chem Eng Sci.* 2005;60(21):5830-5835.
31. Packter A. The precipitation of sparingly soluble alkaline-earth metal and lead salts: nucleation and growth orders during the induction period. *J Chem Soc A.* 1968:859-862.
32. Reddy, MM, Nancollas GH. The crystallization of calcium carbonate: I. Isotopic exchange and kinetics. *J Colloid Interface Sci.* 1971;36(2): 166-172.
33. Marchisio DL, Vigil RD, Fox RO. Implementation of the quadrature method of moments in CFD codes for aggregation-breakage problems. *Chem Eng Sci.* 2003;58:3337-3351.
34. Hounslow MJ, Mumtaz HS, Collier AP, Barrick JP, Bramley AS. A micro-mechanical model for the rate of aggregation during precipitation from solution. *Chem Eng Sci.* 2001;56(7): 2543–2552.
35. Kramer TA, Clark MM. Incorporation of aggregate breakup in the simulation of orthokinetic coagulation. *J. Colloid. Interface Sci.* 1999;216:116–126.
36. Peng SJ, Williams RA. Direct measurement of floc breakage in flowing suspension. *J. Colloid. Interface Sci.* 1994;166:321-332.
37. Garcia-Ochoa F, Gomez E. Theoretical prediction of gas–liquid mass transfer coefficient, specific area and hold-up in sparged stirred tanks. *Chem Eng Sci.* 2004;59:2489–2501.
38. Montante G, Lee KC, Brucato A, Yianneskis M. Numerical simulations of the dependency of flow pattern on impeller clearance in stirred vessels. *Chem Eng Sci.* 2001;56:3751–3770.
39. Gao Z, Li D, Buffo A, Podgorska W, Marchisio DL. Simulation of droplet breakage in turbulent liquid–liquid dispersions with CFD-PBM: Comparison of breakage kernels. *Chem Eng Sci.* 2016;142:277–288.
40. Han B, Qu HY, Nieni H, Sha ZL, Louhi-Kultanen M. Mass transfer and kinetics study of heterogeneous semi-batch precipitation of magnesium carbonate, *Chem Eng Technol.* 2014;37(8):1363-1368.

- 41 Di Veroli G, Rigopoulos. Modeling of turbulent precipitation: A transport population balance-PDF method. *AIChE*. 2010;56(4):878-892.
42. Darmana D, Henket RLB, Deen NG, Kuipers JAM. Detailed modelling of hydrodynamics, mass transfer and chemical reactions in a bubble column using a discrete bubble model: Chemisorption of CO₂ into NaOH solution, numerical and experimental study. *Chem Eng Sci*. 2007;62(9):2556-2575.